



$\text{SrB}_4\text{O}_7:\text{Sm}^{2+}$: an optical sensor reflecting non-hydrostatic pressure at high-temperature and/or high pressure in a diamond anvil cell

Chaoshuai Zhao, Heping Li, Yan Wang, Jianjun Jiang & Yu He

To cite this article: Chaoshuai Zhao, Heping Li, Yan Wang, Jianjun Jiang & Yu He (2016): $\text{SrB}_4\text{O}_7:\text{Sm}^{2+}$: an optical sensor reflecting non-hydrostatic pressure at high-temperature and/or high pressure in a diamond anvil cell, High Pressure Research, DOI: [10.1080/08957959.2016.1269899](https://doi.org/10.1080/08957959.2016.1269899)

To link to this article: <http://dx.doi.org/10.1080/08957959.2016.1269899>



Published online: 20 Dec 2016.



Submit your article to this journal [↗](#)



View related articles [↗](#)



View Crossmark data [↗](#)

SrB₄O₇:Sm²⁺: an optical sensor reflecting non-hydrostatic pressure at high-temperature and/or high pressure in a diamond anvil cell

Chaoshuai Zhao^{a,b}, Heping Li^a, Yan Wang^{a,b}, Jianjun Jiang^{a,b} and Yu He^a

^aKey Laboratory for High-temperature and High-pressure Study of the Earth's Interior, Institute of Geochemistry, Chinese Academy of Sciences, Guiyang, People's Republic of China; ^bCollege of Earth Sciences, University of Chinese Academy of Sciences, Beijing, People's Republic of China

ABSTRACT

A systematic investigation on the fluorescent spectra of SrB₄O₇:Sm²⁺ was performed in detail at high-temperature up to 623 K and/or high pressure up to 23.2 GPa with different pressure-transmitting media (PTMs), respectively. Combined with experiment data of previous research, the change of the ⁷D₀-⁵F₀ line (0-0 line) full width at half maximum (FWHM) of SrB₄O₇:Sm²⁺ under different pressure environments was specifically discussed. The results indicate that the FWHM of 0-0 line is sensitive to the non-hydrostatic pressure environment in 2-propanol, and methanol and ethanol mixture (ME) PTMs at ambient temperature. The first-order and the second-order derivation of the temperature dependence of 0-0 line FWHM at ambient pressure are 1.48 (±0.21) × 10⁻⁴ nm/K and 9.63(±0.63) × 10⁻⁷ nm²/K² below 623 K. The 0-0 line FWHM is also sensitive to the non-hydrostatic pressure environment in ME at high-temperature and high pressure simultaneous, the non-hydrostatic transition pressures are 9.6 GPa at 323 K, 11.0 GPa at 373 K, 14.4 GPa at 423 K, respectively. SrB₄O₇:Sm²⁺ is recommended as an optical sensor to reflect the change of pressure environment in liquid media at high-temperature and/or high pressure.

ARTICLE HISTORY



Received 23 February 2016
Accepted 5 December 2016

KEYWORDS

SrB₄O₇:Sm²⁺; high pressure; high-temperature; non-hydrostatic pressure; FWHM

1. Introduction

Ruby is widely used as a pressure sensor in diamond anvil cells (DACs), because of its convenience, accuracy and rapidity in pressure calibration [1–11]. R₁ fluorescence line of ruby is sensitive to pressure environment, and its FWHM has an obvious change from hydrostatic or quasi-hydrostatic to non-hydrostatic pressure [12–16]. With this property, the change of pressure environment can be easily evaluated and the non-hydrostatic pressure of the liquid medium can be obtained in DACs. This is important to determine the phase diagram and thermodynamic behavior of liquid medium [13,17]. However, this property can be used only at ambient and low temperatures, due to its fatal drawbacks: (1) R₁ line presents a relatively large wavelength shift with temperature, and any error in the

CONTACT Heping Li  liheping@vip.gyig.ac.cn  Key Laboratory for High-temperature and High-pressure Study of the Earth's Interior, Institute of Geochemistry, Chinese Academy of Sciences, 550081 Guiyang, People's Republic of China

temperature measurement will contribute directly to an erroneous determination of pressure [8,10,17]; (2) the line width of R_1 broadens quickly with temperature and the doublet R_1 – R_2 overlaps entirely above 650 K [17], which greatly limits its application as pressure sensor at simultaneous high-temperature and high pressure.

In order to find an optical sensor, whose FWHM is sensitive to non-hydrostatic pressure and insensitive to high-temperature, we focused on a rare-earth-doped material, namely $\text{SrB}_4\text{O}_7:\text{Sm}^{2+}$. Theoretically, the 0–0 line of $\text{SrB}_4\text{O}_7:\text{Sm}^{2+}$ is impervious to temperature, because the shielding of the 4f electrons produces very sharp lines which are less sensitive to the environment compared with the 3d electrons in Cr^{3+} at ruby [1,6,17]. Experimentally, the 0–0 fluorescence line of $\text{SrB}_4\text{O}_7:\text{Sm}^{2+}$ has an isolated, narrow and strong intensity peak at 685.41 nm with a temperature dependence of -1×10^{-4} nm/K below 773 K, and its FWHM is less than 0.30 nm at 650 K. These properties are apparently better than other optical gauges (such as ruby, alexandrite, Sm:MFCl, samarium-doped yttrium aluminum garnet) at simultaneous high-temperature and high pressure [1,4–6,9,10,17].

There were several previous reports about the change of 0–0 line FWHM with pressure environmental transformation at high pressure and/or high-temperature. However, it is still not clear whether 0–0 line FWHM is sensitive to non-hydrostatic pressure or not. Lacam et al. found that the width of 0–0 line was broadened slightly in methanol and ethanol mixture (ME) PTM with an abrupt increase around 10 GPa at ambient temperature [4]. Leger et al. pointed out that in a hydrostatic environment, the width of 0–0 line remained constant with ME mixtures. Under non-hydrostatic conditions, the lines grew broader and induced an overlap between 0–0 and 0–1 emissions [5]. These results probably indicate 0–0 line FWHM is sensitive to non-hydrostatic pressure at ambient temperature. Jing and Datchi et al. put forward that the singlet character of 0–0 line kept at Mbar without overlap under non-hydrostatic pressure [1,9], which is contrary to the result described by Leger et al. [5]. Datchi et al. also pointed out that the pressure response of 0–0 line was weakly dependent on non-hydrostaticity of PTM [1]. Rashchenko et al. found that the FWHM of 0–0 line gradually increased with pressure up to 60 GPa [18]. These results may directly or indirectly show 0–0 line FWHM is insensitive to non-hydrostatic pressure. In addition, Lacam et al. investigated the width of 0–0 line at four fixed pressures with thermal cycle to 573 K and found that the FWHM was reduced to a minimum ('hydrostatic') value at a sufficient temperature [19], which presents that temperature effect can improve the pressure environment. However, there is no direct proof to reflect whether the FWHM of 0–0 line is sensitive to non-hydrostatic pressure at simultaneous high-temperature and high pressure. Therefore, in this study, we systematically investigated the FWHM of 0–0 line as a function of pressure and/or temperature individually. Other spectral parameters of $\text{SrB}_4\text{O}_7:\text{Sm}^{2+}$ are also presented in detail in this work. Compared with the results of a previous and this study, the effect of non-hydrostatic pressure and fluorescent spectra of $\text{SrB}_4\text{O}_7:\text{Sm}^{2+}$ is thoroughly discussed.

2. Experiment

In the current work, powdered samples of $\text{SrB}_4\text{O}_7:\text{Sm}^{2+}$ was synthesized by the high-temperature solid state reactions in air. Stoichiometric amounts of the strontium carbonate (purity 99.99%), samarium oxide (purity 99.99%) and boric acid (excess 6 w %, purity

99.8%) were mixed homogeneously. The mixtures were heated at 700 °C in a corundum crucible for 5 h, which was similar to the method by Mikhail [20]. A second annealing step was necessary at 850 °C for 24 h and repeated twice in order to accomplish the reactions. Then the mixtures were heated at 950 °C in a yttria-stabilized zirconia (YSZ) crucible for 24 h and repeated twice. Finally, the $\text{SrB}_4\text{O}_7\text{:Sm}^{2+}$ powder was obtained. The X-ray diffraction analysis revealed that a small amount of SrB_3O_6 was presented in this compound [21]. The minor phase was also found by Sakirza-novas et al. with the same method [22].

High pressure was generated by a cell with two opposed diamond anvils and a T301 stainless steel as gaskets. The culets of anvils were 400 μm . The initial thicknesses of gaskets were preindented from 250 to ~ 65 μm . Spectrographic grade methanol and ethanol (purity no less than 99.9% and 99.8%, respectively) mixture (volume ratio 4:1) and 2-propanol (purity no less than 99.5%, both from Aladdin company) were applied as PTMs. $\text{SrB}_4\text{O}_7\text{:Sm}^{2+}$ (finely ground powder, grain size less than 5 μm) and ruby (single crystal grain, 1–15 μm) were placed in ~ 160 μm diameter holes processed by a laser drilling machine. In order to obtain a reliable comparison between their pressure shifts, the spectra of the two sensors were measured at the same position in the sample chamber. For high-temperature experiments, the sample chamber was heated by external resistance heating with two separate resistive furnaces (method similar to Raju et al. [8]). Temperature was measured by an R/S type platinum–rhodium and platinum thermocouple (Omega technology company, America) with the precision of ± 1 K in our experimental temperature range. The tip of thermocouple was cemented at an anvil close to the culet with 940HT glue. The thermocouple was used for temperature measurement and stabilization through a feedback loop in the temperature controller (CN3251, Omega technology company). We elevated 25 K each time and maintained 5 min to guarantee the stabilization and uniformity of temperature in sample chamber and the change displayed at controller's panel was less than ± 1 K. We measured the fluorescent spectra of $\text{SrB}_4\text{O}_7\text{:Sm}^{2+}$ each 25 K up to 623 K at ambient pressure and to 573 K at high pressure, respectively. Spectrum measurements were conducted on a Renishaw 2000 micro-confocal laser Raman spectrometer equipped with a charge-coupled device (CCD) detector, a 2400 lines/mm diffraction grating and a holographic notch filter. The samples were excited with a laser beam which was around ~ 5 μm in diameter at the focus with an Olympus microscope 20 \times ultra-length working distance objective [23]. Scattered radiation was collected through backscattering. The spectrum physics model of 2017 argon ion laser operating at 514.5 nm was used as the excitation source, and the laser power used was 80 mW with 5% (namely 4 mW) at high pressure and 40 mW with 0.1% (namely 0.04 mW) at high-temperature. The Raman spectrometer was calibrated by single crystal silicon at 520.0 cm^{-1} before experiments. The fluorescent spectra of ruby and $\text{SrB}_4\text{O}_7\text{:Sm}^{2+}$ were measured in the range from 675 to 715 nm at high pressure and/or high-temperature, respectively. To test the repeatability of the results, experiments with different loading sample were conducted and run twice independently. The spectrum was recorded at pressure up to 23.2 GPa and temperature to 623 K. Pressures were determined by the quasi-hydrostatic ruby scale [11]. The wavelength positions of fluorescence peaks, FWHM and intensity were acquired by spectral analysis software Renishaw WiRe 4.1 and fitted with the Gaussian–Lorentz mixed curve. The instrumental resolution was 1 cm^{-1} .

3. Result and discussion

3.1. High pressure and ambient temperature

In our pressure range, the ruby peaks (R_1) almost overlap with 0–1–1 line of $\text{SrB}_4\text{O}_7:\text{Sm}^{2+}$, which enormously affects the accuracy of FWHM of ruby R_1 , so the FWHM of ruby R_1 and 0–0 line is not shown simultaneously here. In addition, in order to ensure the precision and reliability, the experiments with different loading samples and PTMs are performed independently, and the results are well consistent with each other.

It is known that the FWHM of ruby R_1 is sensitive to non-hydrostatic pressure, and it usually has a big change when the pressure environment worsens sharply. If the accordant phenomenon is found at the 0–0 line FWHM, then it can account for that the $\text{SrB}_4\text{O}_7:\text{Sm}^{2+}$ sensor is sensitive to pressure environment. In this study, the 0–0 line FWHM of $\text{SrB}_4\text{O}_7:\text{Sm}^{2+}$ as a function of pressure at ambient temperature is shown in Figure 1. Two dependent experimental results are presented indicating that the transition pressures of the 0–0 line FWHM are 4.0 GPa in 2-propanol and 9.6 GPa in ME, respectively, which are in good agreement with the glass transition pressure at ~ 4.2 and ~ 10.0 GPa, respectively, by a previous study [12,14,24,25]. In addition, Piermarini et al. pointed that the line width of ruby increased dramatically as pressure exceeded the glass transition of the liquid material, it also demonstrated definitely the non-hydrostatic character of the material

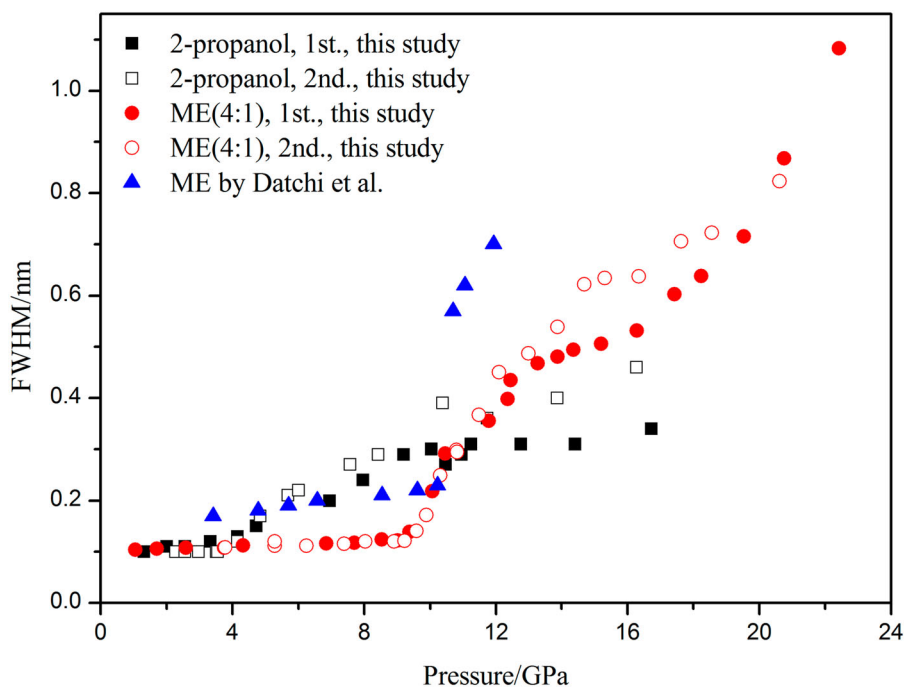


Figure 1. The 0–0 line FWHM of $\text{SrB}_4\text{O}_7:\text{Sm}^{2+}$ as a function of pressure at ambient temperature. Solid red circles and open red circles: the first and second experiment data of $\text{SrB}_4\text{O}_7:\text{Sm}^{2+}$ within ME PTM; solid black squares and open black squares: the first and second experiment data of $\text{SrB}_4\text{O}_7:\text{Sm}^{2+}$ within 2-propanol PTM, in this study; solid blue up triangles: $\text{SrB}_4\text{O}_7:\text{Sm}^{2+}$ data from Lacam et al. (1989) within ME PTM.

[12]. As we can see in Figure 1, the 0–0 line FWHM changes obviously at the pressure of glass transition in 2-propanol and ME PTMs and it is more obvious in the latter. Therefore, the $\text{SrB}_4\text{O}_7:\text{Sm}^{2+}$ as an optical sensor can be used to reflect non-hydrostatic pressure environment at ambient temperature and high pressure. For convenience, we considered the transition pressure of the 0–0 line FWHM as non-hydrostatic transition pressure thereafter.

The characteristic of FWHM of 0–0 line is described in detailed here. Below the non-hydrostatic pressure within ME PTM, the FWHM of 0–0 line change with pressure can be described as follows:

$$\Gamma_{0-0}(P) = 0.102(\pm 0.001) + 2.29(\pm 0.20) \times 10^{-3} P, \quad (1)$$

where the FWHM of 0–0 line at ambient temperature and ambient pressure is 0.102 nm. $\Gamma_{0-0}(P)$ is the FWHM of 0–0 line at high pressure and P in GPa and Γ in nm. The FWHM of 0–0 line at two independent experiments are almost constant and change from 0.10 to 0.14 nm at pressure below 9.6 GPa. It reflects the homogenous pressure environment. The slope of 0–0 line FWHM by pressure ($\partial\Gamma_{0-0}/\partial P$) is 2.29×10^{-3} nm/GPa, which is a quarter to the value 8.0×10^{-3} nm/GPa obtained by Lacam et al., who found that the FWHM of 0–0 line increased slowly near 0.22 nm below 10 GPa [19]. Above 9.6 GPa, the FWHM increases dramatically at the beginning. Around 15 GPa, the increase reduces a little, this phenomenon may be caused by a slight pressure release from the expansion of the gasket hole. Then the FWHM increases quickly again at higher pressure, and the slope $\partial\Gamma_{0-0}/\partial P$ is also near to a quarter of the value by Lacam et al. [19]. In conclusion, the obvious variation of line width at critical pressure indicates that the FWHM of 0–0 line is quite sensitive to non-hydrostatic pressure.

3.2. High-temperature and ambient pressure

The fluorescent spectra of $\text{SrB}_4\text{O}_7:\text{Sm}^{2+}$ at high-temperature up to 623 K and ambient pressure are obtained. Higher temperature is unnecessary for the quick decrease in the signal-to-noise ratio. The linear fitting results of 0–0 line wavelength shift with temperature ($\partial\lambda_{0-0}/\partial T$) is $-9.74(\pm 0.48) \times 10^{-5}$ nm/K, which is in agreement with the data (-1×10^{-4} nm/K) in references [1,4,17]. At 623 K, the blue shift is only 0.03 nm, which can be neglected within the error range. In addition, the slope of 0–1 lines $\partial\lambda_{0-1}/\partial T$ are $8.27(\pm 0.10) \times 10^{-4}$, $-3.54(\pm 0.06) \times 10^{-4}$, $5.75(\pm 1.15) \times 10^{-5}$ nm/K, respectively. All of these slopes are almost less than the values measured by Lacam et al. [4].

The FWHM of $\text{SrB}_4\text{O}_7:\text{Sm}^{2+}$ as a function of temperature is shown in Figure 2 and Table 1. The second-order polynomial fitting of 0–0 and 0–1 lines is displayed as follows:

$$\Gamma_{0-0}(T) = 0.102(0.002) + 1.48(0.21) \times 10^{-4}(T - 298) + 9.63(0.63) \times 10^{-7}(T - 298)^2, \quad (2)$$

$$\Gamma_{0-1-1}(T) = 0.272(0.005) + 6.44(0.79) \times 10^{-4}(T - 298) + 9.94(2.55) \times 10^{-7}(T - 298)^2, \quad (3)$$

$$\Gamma_{0-1-2}(T) = 0.240(0.007) + 6.39(1.10) \times 10^{-4}(T - 298) + 8.92(3.52) \times 10^{-7}(T - 298)^2, \quad (4)$$

$$\Gamma_{0-1-3}(T) = 0.590(0.034) + 7.74(4.87) \times 10^{-4}(T - 298) + 5.05(1.44) \times 10^{-6}(T - 298)^2, \quad (5)$$

where the 0–0 line FWHM at 298 K is 0.102 nm. $\Gamma_{0-0}(T)$ is the 0–0 line FWHM at high-temperature, $\Gamma_{0-1-i}(T)$ is the FWHM of 0–1 line at high-temperature, in which $i = 1, 2, 3$, T in kelvin

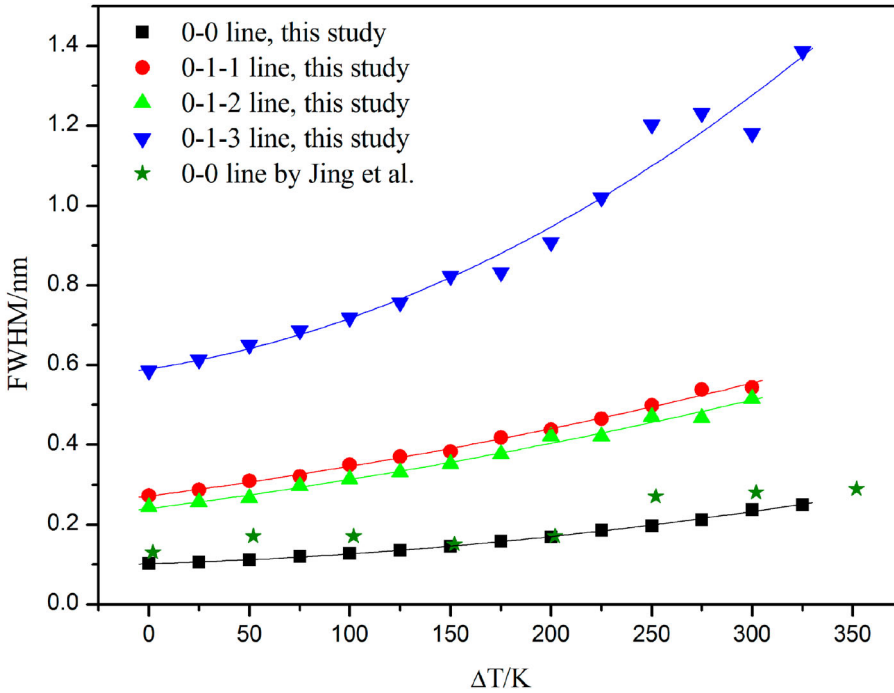


Figure 2. The 0–0 and 0–1 lines FWHM of $\text{SrB}_4\text{O}_7:\text{Sm}^{2+}$ as a function of temperature at ambient pressure. $\Delta T = T - 298$ K, solid black squares: 0–0 line; solid red spheres: 0–1–1 line; solid green up triangle: 0–1–2 line; solid blue down triangle: 0–1–3 line; solid olive star: 0–0 line by Jing et al. (2013). Solid black line: second-order polynomial fit of 0–0 line, formula (2), $R^2 = 0.998$; solid red line: second-order polynomial fit of 0–1–1 line, formula (3), $R^2 = 0.994$; solid green line: second-order polynomial fit of 0–1–2 line, formula (4), $R^2 = 0.988$; solid blue line: second-order polynomial fit of 0–1–3 line, formula (5), $R^2 = 0.965$.

Table 1. Parameters determined in a curve fit of the equation for the 0–0 and 0–1 lines of $\text{SrB}_4\text{O}_7:\text{Sm}^{2+}$.

| Transitions | Wavelength (nm) | $d\lambda/dT$ (nm/K) | $d\Gamma/dT$ (nm/K) | $d^2\Gamma/d^2T$ (nm ² /K ²) |
|--|-----------------|-------------------------------|------------------------------|---|
| $^5\text{D}_0\text{--}^7\text{F}_0(0\text{--}0)$ | 685.38 | $-9.74 (0.48) \times 10^{-5}$ | $1.48 (0.21) \times 10^{-4}$ | $9.63 (0.63) \times 10^{-7}$ |
| $^5\text{D}_0\text{--}^7\text{F}_1(0\text{--}1)$ | 695.47 | $8.27 (0.10) \times 10^{-4}$ | $6.44 (0.79) \times 10^{-4}$ | $9.94 (2.55) \times 10^{-7}$ |
| | 698.64 | $-3.54 (0.06) \times 10^{-4}$ | $6.39 (1.10) \times 10^{-4}$ | $8.92 (3.52) \times 10^{-7}$ |
| | 704.64 | $5.75 (1.15) \times 10^{-5}$ | $7.74 (4.87) \times 10^{-4}$ | $5.05 (1.44) \times 10^{-6}$ |

and Γ in nm. At 473 K, the change of FWHM of 0–0 line is only 0.05 nm. At 623 K, the result is 0.15 nm, which is similar to the result of Jing et al. [4,10]. Moreover, the temperature dependence of 0–1 lines FWHM is also presented. The increase of 0–1–1 and 0–1–2 line FWHM with temperature is almost the same. Their change is 0.27 nm at 598 K. The FWHM of 0–1–3 line changes obviously (0.80 nm at 623 K), which is not suitable for pressure calibration at high-temperature.

3.3. High-temperature and high pressure

The 0–0 line FWHM of $\text{SrB}_4\text{O}_7:\text{Sm}^{2+}$ is comparatively complex under high-temperature and high pressure simultaneous. Pressure effect is simple, FWHM increases as a function of

pressure, especially dramatically increasing above a critical pressure. Temperature effect is complex, on the one hand, FWHM increases slowly as a function of temperature. On the other hand, it may decrease to a ‘hydrostatic’ value at a sufficient temperature [19]. The 0–0 line FWHM at simultaneous high-temperature and high pressure with ME as PTM is shown in Figure 3 and Table 2. The 0–0 line FWHM almost maintains to a constant value at different temperatures of 323, 373, 423, 473, 523, 573 K below the critical pressure (see those arrows in Figure 3), and a suddenly increasing FWHM is observed at 323, 373, 423 K above the pressure. This phenomenon is similar to the observation at ambient temperature and high pressure as described in Figure 1, which reflects that 0–0 line FWHM is also sensitive to the non-hydrostatic pressure at simultaneous high-temperature and high pressure. The non-hydrostatic transition pressure is 9.6 GPa at 323 K. It is almost equal to the value at 293 K within correction. At 373 and 423 K, the pressures are 11.0 and 14.4 GPa, respectively. Above 423 K, the value is higher beyond the pressure range of this study. The transition pressure of ME is found to increase non-linearly with temperature. It is the first time that the non-hydrostatic transition pressure of ME at high-temperature (323, 373, 423 K) is reported by this method.

The initial FWHM Γ_0 fitting from high-temperature and high pressure data is nearly equal to the measured value Γ^*_0 at high-temperature and ambient pressure within

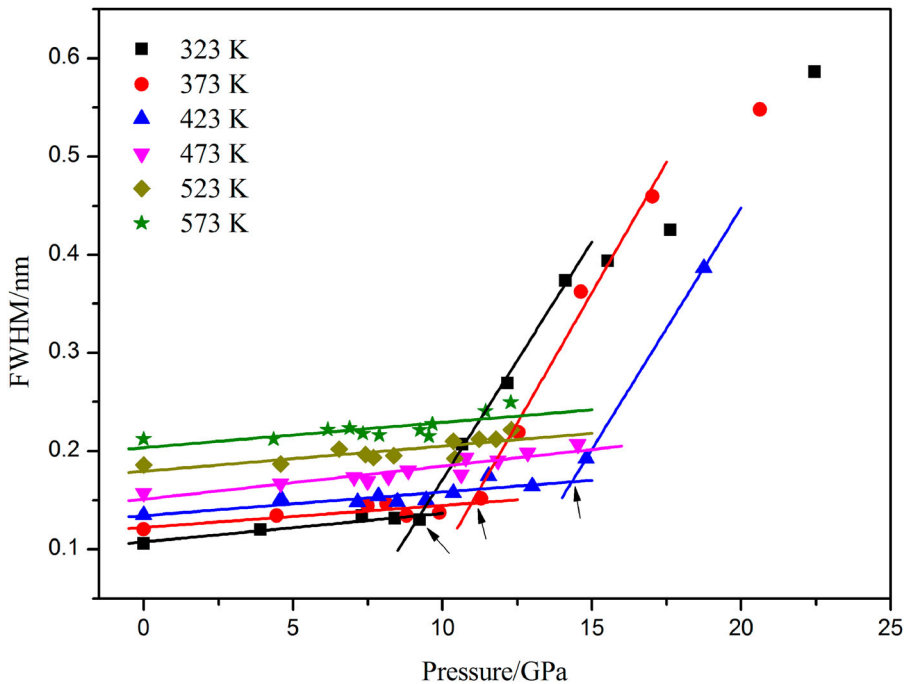


Figure 3. The 0–0 line FWHM of $\text{SrB}_4\text{O}_7:\text{Sm}^{2+}$ as a function of temperature and pressure simultaneous in ME PTM. The symbols represent data collected at the following temperatures: ■ FWHM at 323 K; ● FWHM at 373 K; ▲ FWHM at 423 K; ▼ FWHM at 473 K; ◆ FWHM at 523 K; ★ FWHM at 573 K; solid black line: linear fit of 0–0 line FWHM at 323 K; solid red line: linear fit of 0–0 line FWHM at 373 K; solid blue line: linear fit of 0–0 line FWHM at 423 K; solid magenta line: linear fit of 0–0 line FWHM at 473 K; solid dark yellow line: linear fit of 0–0 line FWHM at 523 K; solid olive line: linear fit of 0–0 line FWHM at 573 K; the arrows show the non-hydrostatic pressure.

Table 2. The parameters of FWHM of 0–0 line as a function of pressure at each thermal cycle.

| Condition Temperature (K) | FWHM | | | Hydrostatic ^a $\partial\Gamma/\partial P$ (nm/GPa) | Non-hydrostatic ^b $\partial\Gamma/\partial P$ (nm/GPa) |
|------------------------------|----------------------|-------------------|-----------------------------------|--|--|
| | Γ_0^{*c} (nm) | Γ_0^d (nm) | $\Gamma_0^d - \Gamma_0^{*c}$ (nm) | | |
| 293 | 0.102 | 0.102 (0.001) | 0.000 | 2.29 (0.20) $\times 10^{-3}$ | 5.43 (0.37) $\times 10^{-2}$ |
| 323 | 0.106 | 0.108 (0.004) | 0.002 | 2.90 (0.55) $\times 10^{-3}$ | 4.83 (0.38) $\times 10^{-2}$ |
| 373 | 0.121 | 0.122 (0.005) | 0.001 | 2.24 (0.67) $\times 10^{-3}$ | 5.32 (0.79) $\times 10^{-2}$ |
| 423 | 0.135 | 0.134 (0.005) | −0.001 | 2.40 (0.59) $\times 10^{-3}$ | 4.92 (0.63) $\times 10^{-2}$ |
| 473 | 0.158 | 0.151 (0.005) | −0.007 | 3.38 (0.47) $\times 10^{-3}$ | – |
| 523 | 0.186 | 0.180 (0.006) | −0.006 | 2.57 (0.65) $\times 10^{-3}$ | – |
| 573 | 0.212 | 0.204 (0.006) | −0.008 | 2.55 (0.77) $\times 10^{-3}$ | – |

^aBelow non-hydrostatic pressure, the linear fitting pressure range shown by Figure 3.

^bAbove non-hydrostatic pressure, the linear fitting pressure range shown by Figure 3.

^c Γ_0^* , the measured FWHM at high-temperature and ambient pressure.

^d Γ_0^d , the initial value of FWHM calculated from the FWHM at high-temperature and high pressure simultaneous.

correction. The calculated values are 0.108 nm at 323 K, 0.122 nm at 373 K, 0.134 nm at 423 K, 0.151 nm at 473 K, 0.180 nm at 523 K and 0.204 nm at 573 K, which are nearly equivalent to the measured values 0.106, 0.121, 0.135, 0.158, 0.186, 0.212 nm, respectively (see Table 2). In addition, the pressure dependence of 0–0 lines FWHM $\partial\Gamma/\partial P$ is 2.90×10^{-3} at 323 K, 2.24×10^{-3} at 373 K, 2.40×10^{-3} at 423 K, 3.38×10^{-3} at 473 K, 2.57×10^{-3} at 523 K, 2.55×10^{-3} at 573 K nm/GPa below non-hydrostatic pressure, respectively. These results are nearly concordant with the value 2.29×10^{-3} nm/GPa at 293 K. Above the non-hydrostatic pressure, in the beginning, the pressure dependence of 0–0 lines FWHM $\partial\Gamma/\partial P$ is 4.83×10^{-2} nm/GPa at 323 K, 5.32×10^{-2} nm/GPa at 373 K and 4.92×10^{-2} nm/GPa at 423 K. These results are nearly concordant with the value 5.43×10^{-2} nm/GPa at 293 K (see Figure 3 and Table 2). Obviously, 0–0 line FWHM as a function of pressure has a similar pattern between high-temperature and high pressure and ambient temperature and high pressure, which further verifies our conclusion.

Based on the description above, the 0–0 line FWHM of $\text{SrB}_4\text{O}_7:\text{Sm}^{2+}$ can be used to reflect the non-hydrostatic pressure at high-temperature and high pressure simultaneously. However, Datchi et al. observed that the $\text{SrB}_4\text{O}_7:\text{Sm}^{2+}$ was dissolved by liquid water at 650 K and 8.5 GPa and by the equimolar $\text{HF}:\text{H}_2\text{O}$ liquid sample above ~ 400 K [17]. It also should be noted that $\text{SrB}_4\text{O}_7:\text{Sm}^{2+}$ may be not appropriate to reflect the non-hydrostatic pressure in neon and helium based on the results of ruby R_1 by Klotz et al. [25] and $\text{SrB}_4\text{O}_7:\text{Sm}^{2+}$ by Rashchenko et al. [18].

4. Conclusion

The 0–0 fluorescence line of $\text{SrB}_4\text{O}_7:\text{Sm}^{2+}$ is fully investigated at temperature up to 623 K and/or pressure up to 23.2 GPa, respectively. Some critical conclusions are found and presented: (1) the 0–0 line FWHM of $\text{SrB}_4\text{O}_7:\text{Sm}^{2+}$ is sensitive to non-hydrostatic pressure environment at high pressure and ambient temperature; (2) compared with the influence of non-hydrostatic pressure, the influence of temperature (at ambient pressure) on the change of the 0–0 line FWHM can be ignored; (3) the change of 0–0 line FWHM is obvious under a certain temperature and pressure at high-temperature and high pressure simultaneous. Combined with the experimental data of this study and previous work, $\text{SrB}_4\text{O}_7:\text{Sm}^{2+}$ is recommended as an optical sensor reflecting non-hydrostatic pressure at high-temperature/high pressure in liquid media, which is better than traditional pressure gauge: ruby.

Acknowledgements

The authors of the work extend thanks to Prof. Changsheng Zha for the guidance and advice on the experiment, and Dr Lin Chen for the guidance of Raman technology.

Disclosure statement

No potential conflict of interest was reported by the authors.

Funding

The authors acknowledge the support of 135 project of Institute of Geochemistry, Chinese Academy of Sciences, National Natural Science Foundation of China (grant no. 51302259).

References

- [1] Datchi F, LeToullec R, Loubeyre P. Improved calibration of the $\text{SrB}_4\text{O}_7\text{:Sm}^{2+}$ optical pressure gauge: advantages at very high pressures and high temperatures. *J Appl Phys.* **1997**;81(8):3333–3339.
- [2] Chijioke AD, Nellis WJ, Soldatov A, et al. The ruby pressure standard to 150 GPa. *J Appl Phys.* **2005**;98(11):114905-1–114905-9.
- [3] Yamaoka H, Zekko Y, Jarrige I, et al. Ruby pressure scale in a low-temperature diamond anvil cell. *J Appl Phys.* **2012**;112(12):124503-1–124503-5.
- [4] Lacam A, Chateau C. High-pressure measurements at moderate temperatures in a diamond anvil cell with a new optical sensor: $\text{SrB}_4\text{O}_7\text{:Sm}^{2+}$. *J Appl Phys.* **1989**;66(1):366–372.
- [5] Leger JM, Chateau C, Lacam A. $\text{SrB}_4\text{O}_7\text{:Sm}^{2+}$ pressure optical sensor: investigations in the megabar range. *J Appl Phys.* **1990**;68(5):2351–2354.
- [6] Goncharov AF, Zaug JM, Crowhurst JC, et al. Optical calibration of pressure sensors for high pressures and temperatures. *J Appl Phys.* **2005**;97(9):094917-1–094917-5.
- [7] Syassen K. Ruby under pressure. *High Press Res.* **2008**;28(2):75–126.
- [8] Raju SV, Zaug JM, Chen B, et al. Determination of the variation of the fluorescence line positions of ruby, strontium tetraborate, alexandrite, and samarium-doped yttrium aluminum garnet with pressure and temperature. *J Appl Phys.* **2011**;110(2):023521-1–023521-5.
- [9] Jing QM, Wu Q, Liu L, et al. An experimental study on $\text{SrB}_4\text{O}_7\text{:Sm}^{2+}$ as a pressure sensor. *J Appl Phys.* **2013**;113(2):023507-1–023507-5.
- [10] Jing QM, Wu Q, Liu YG, et al. Effect of pressure and temperature on the wavelength shift of the fluorescence line of $\text{SrB}_4\text{O}_7\text{:Sm}^{2+}$ scale. *High Press Res.* **2013**;33(4):725–733.
- [11] Mao HK, Xu JA, Bell PM. Calibration of the ruby pressure gauge to 800 kbar under quasi-hydrostatic conditions. *J Geophys Res.* **1986**;91(5):4673–4676.
- [12] Piermarini GJ, Block S, Barnett JD. Hydrostatic limits in liquids and solids to 100 kbar. *J Appl Phys.* **1973**;44(12):5377–5382.
- [13] Iizuka R, Kagi H, Komatsu K. Comparing ruby fluorescence spectra at high pressure in between methanol-ethanol pressure transmitting medium and its deuteride. *J Phys.* **2010**;215(1):012177-1–02177-5.
- [14] Wang XB, Shen ZX, Tang SH, et al. Near infrared excited micro-Raman spectra of 4:1 methanol-ethanol mixture and ruby fluorescence at high pressure. *J Appl Phys.* **1999**;85(12):8011–8017.
- [15] Tateiwa N, Haga Y. Appropriate pressure-transmitting media for cryogenic experiment in the diamond anvil cell up to 10 GPa. *J Phys.* **2010**;215(1):012178-1–021178-7.
- [16] Bassett WA. Diamond anvil cell, 50th birthday. *High Press Res.* **2009**;29(2):163–186.
- [17] Datchi F, Dewaele A, Loubeyre P, et al. Optical pressure sensors for high-pressure-high-temperature studies in a diamond anvil cell. *High Press Res.* **2007**;27(4):447–463.
- [18] Rashchenko SV, Kurnosov A, Dubrovinsky L, et al. Revised calibration of the $\text{Sm}\text{:Sr-B}_4\text{O}_7$ pressure sensor using the Sm-doped yttrium-aluminum garnet primary pressure scale. *J Appl Phys.* **2015**;117(14):125902-1–125902-5.

- [19] Lacam A. The $\text{SrB}_4\text{O}_7:\text{Sm}^{2+}$ optical sensor and the pressure homogenization through thermal cycles in diamond anvil cells. *High Press Res.* **1990**;5:782–784.
- [20] Mikhail P, Hulliger J, Schnieper M, *et al.* $\text{SrB}_4\text{O}_7:\text{Sm}^{2+}$: crystal chemistry, Czochralski growth and optical hole burning. *J Mater Chem.* **2000**;10:987–991.
- [21] Wang Y. Synthesis and characterization of a new hauge: $\text{Sr}_{1-x}\text{Sm}_x\text{B}_4\text{O}_7$ [dissertation]. Guiyang: Institute of Geochemistry, Chinese Academy of Sciences; 2016.
- [22] Sakirzanovas S, Katelnikovas A, Dutczak D, *et al.* Concentration influence on temperature dependent luminescence properties of samarium substituted strontium tetraborate. *J Lumin.* **2012**;132:141–146.
- [23] Gao R, Li HP. Pressure measurement using the R fluorescence peaks and 417 cm^{-1} Raman peak of an anvil in a sapphire-anvil cell. *High Press Res.* **2012**;32(2):1–10.
- [24] Tateiwa N, Haga Y. Evaluations of pressure-transmitting media for cryogenic experiments with diamond anvil cell. *Rev Sci Instrum.* **2009**;80(12):123901-1–123901-7.
- [25] Klotz S, Chervin JC, Munsch P, *et al.* Hydrostatic limits of 11 pressure transmitting media. *J Phys D: Appl Phys.* **2009**;42:075413-1–075413-7.